Picosecond Time-Resolved X-Ray Absorption Spectroscopy of Ultrafast Aluminum Plasmas

P. Audebert,[1] P. Renaudin,[2] S. Bastiani-Ceccotti,[1] J.-P. Geindre,[1] C. Chenais-Popovics,[1] S. Tzortzakis,[1] V. Nagels-Silvert,[1]
R. Shepherd,[3] I. Matsushima,[4] S. Gary,[2] F. Girard,[2] O. Peyrusse,[5] and J.-C. Gauthier[5]

[1]*Laboratoire pour l'Utilisation des Lasers Intenses (LULI), UMR 7605, CNRS-CEA-Université Paris VI-Ecole Polytechnique,
91128 Palaiseau, France*
[2]*Commissariat à l'Energie Atomique, B.P. 12, 91680 Bruyères-le-Châtel, France*
[3]*Lawrence Livermore National Laboratory, University of California, Livermore, California 94550, USA*
[4]*National Institute of Advanced Industrial Science and Technology (AIST), Umezono, Tsukuba, 3058568, Japan*
[5]*Centre Lasers Intenses et Applications, UMR 5107, CNRS-CEA-Université Bordeaux 1, 33405 Talence, France*
(Received 15 September 2004; published 18 January 2005)

We have used point-projection *K*-shell absorption spectroscopy to infer the ionization and recombination dynamics of transient aluminum plasmas. Two femtosecond beams of the 100 TW laser at the LULI facility were used to produce an aluminum plasma on a thin aluminum foil (83 or 50 nm), and a picosecond x-ray backlighter source. The short-pulse backlighter probed the aluminum plasma at different times by adjusting the delay between the two femtosecond driving beams. Absorption x-ray spectra at early times are characteristic of a dense and rather homogeneous plasma. Collisional-radiative atomic physics coupled with hydrodynamic simulations reproduce fairly well the measured average ionization as a function of time.

Plasma formation by intense laser irradiation of solids provides a unique opportunity to investigate x-ray emission properties of dense plasmas in transient local thermodynamic equilibrium (LTE). These plasmas can be found in many fields of applied and fundamental research, in the development of laser-plasma sources and x-ray lasers [1], the study of plasmas for inertial confinement fusion [2], and laboratory astrophysics [3]. Also, x-ray emission from these plasmas is used for benchmarking kinetic codes [4], provided that plasma parameters are measured in detail. Recent advances in ultrashort-pulse laser technology have allowed one to create highly transient plasmas where the ionization-recombination dynamics time scale is comparable to or longer than the laser pulse duration. Additionally, when a subpicosecond laser pulse irradiates a very thin foil ($\approx$ tens of nm) with intensities in the range of 10^{15}–10^{16} W/cm^2, impulse heating followed by rapid heat conduction produces a high-density, medium-temperature plasma with minimal hydrodynamic expansion [5] and longitudinal gradients [6].

Point-projection absorption spectroscopy based on the use of short-pulse x-ray backlighter sources is a powerful diagnostic of ionization of low temperature plasmas [7]. X-ray sources of a few picosecond duration emitting in the sub-5-keV range have proven to be feasible by irradiating high-*Z* materials with a subpicosecond laser pulse [8]. In recent experiments ultrashort laser pulses have been used for picosecond point-projection spectroscopy of nanosecond laser-produced expanding plasmas [9], providing space- and time-resolved information on the average ionization. This opens the way to infer ion charge state distributions directly, with a time resolution commensurable with the ionization time scale. In this Letter, we present the long-awaited experimental realization of this idea, using

two ultrafast lasers to produce both the plasma and the x-ray probe. A first ultrashort laser pulse created a thin, high-density plasma slab fairly uniform in density and temperature. An ultrashort x-ray pulse, produced by the second ultrashort laser beam, was used to backlight the slab. Single-shot frequency domain interferometry (FDI) was independently used to probe the time-resolved expansion of the plasma.
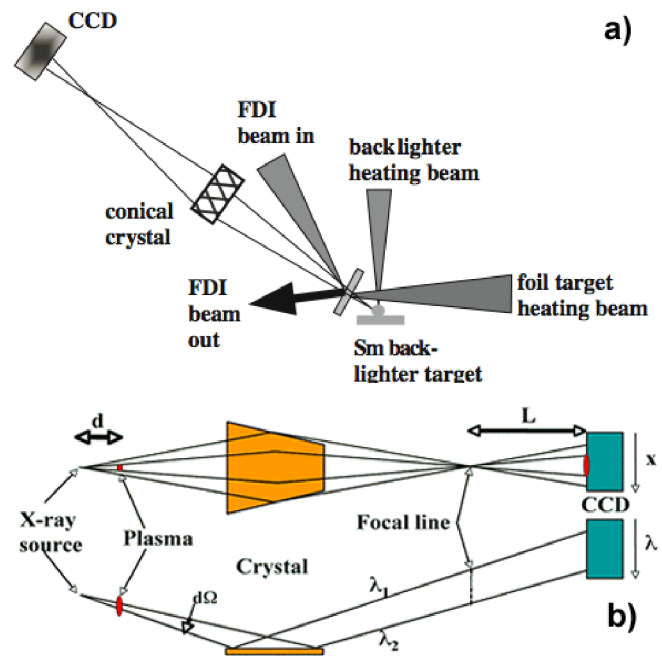
FIG. 1 (color online). Experimental setup. (a) Layout of the different laser beams. (b) Top and side views of the conically bent crystal spectrograph; $L = 90$ mm, $d = 3$ mm.

The experiment was performed at the LULI facility, using two 300-fs laser beams set as shown in Fig. 1(a). A 0.3-J (1.06-μm) beam heated a 50- or 83-nm thick aluminum layer, deposited on a self-standing 25-nm silicon nitride (Si_3N_4) substrate. This membrane supported a 300-μm diameter gold pinhole made of a 0.5-μm thick Au deposit to limit the plasma region viewed by the diagnostics. The p-polarized heating beam was focused at a 15° incidence angle on the Si_3N_4 side of the target, limiting the longitudinal gradients in aluminum. The measured prepulse intensity contrast ratio was 10^{-7}. The focal spot was elliptic, 180 μm in the plane of incidence and 60 μm in the perpendicular direction (see Fig. 1). A 5-J energy (0.53-μm) beam focused on a samarium sample with an off-axis parabola to a spot size of 20 μm produced the backlighter. The peak laser intensity was 2×10^{17} W/cm^2. Diagnostics were viewing the rear side of the target, i.e., the thin Al layer side. A single-shot FDI diagnostic system [10] monitored the phase of a chirped probe laser beam (1.06 μm) of 15-ps duration, reflected at a 47° incidence angle on the rear critical surface of the plasma [see Fig. 1(a)]. X-ray transmission spectra were recorded with a conically bent potassium-hydrogen-phthalate crystal spectrometer [11], with a resolving power $E/\Delta E = 1000$, coupled to a cooled 1024×1024 16-bits charge-coupled device (CCD) camera. The 7.7–8.5 Å spectral region covered the Al^{4+} to Al^{11+} inner shell $n = 1$ to 2 transitions and the Al^{3+} and Al^{4+} $n = 1$ to 3 transitions. For the spectral region studied here, the Sm plasma pro-

vided a 4-ps duration quasicontinuum backlighter spectrum [8]. For point-projection spectroscopy, the conically bent crystal spectrograph allowed magnification adjustments by moving the detector away from the focal line of the imaging crystal, without changing the wavelength range. The spectra were recorded with a magnification of 30 by setting the CCD camera at $L = 90$ mm beyond the focus of the crystal and the backlighter source at $d = 3$ mm from the plasma [see Fig. 1(b)].

Figure 2 shows space-resolved absorption spectra at different times after the heating laser in the case of the (a) 83-nm and (b) 50-nm foil irradiated at a laser intensity of 3×10^{15} W/cm^2. For the 83-nm case, the plasma recombination is seen to be fast, with a stagnation phase between 7 and 15 ps. For the 50-nm thick foil, higher ionic stages are observed compared to the 83-nm thick foil case. The low charge states (Al^{4+} and Al^{5+}) disappear in the middle of the focal spot, where the laser intensity is larger and the plasma hotter. The image measured at 7 ps for the 83-nm foil is particularly interesting. At shorter wavelengths, Al^{3+} and Al^{4+} $1s$-$3p$ absorption lines can be seen on the edge of the focal spot at 7.883 and 7.741 Å, respectively. Also, the cold aluminum K edge, at 7.95 Å, is visible outside the focal spot. The absolute transmission near the K edge was used to check the initial foil density and thickness provided by the manufacturer.

The electron temperature at the peak of the laser pulse was deduced from the FDI diagnostic system. Indeed, the phase shift of the reflected light depends mainly on the
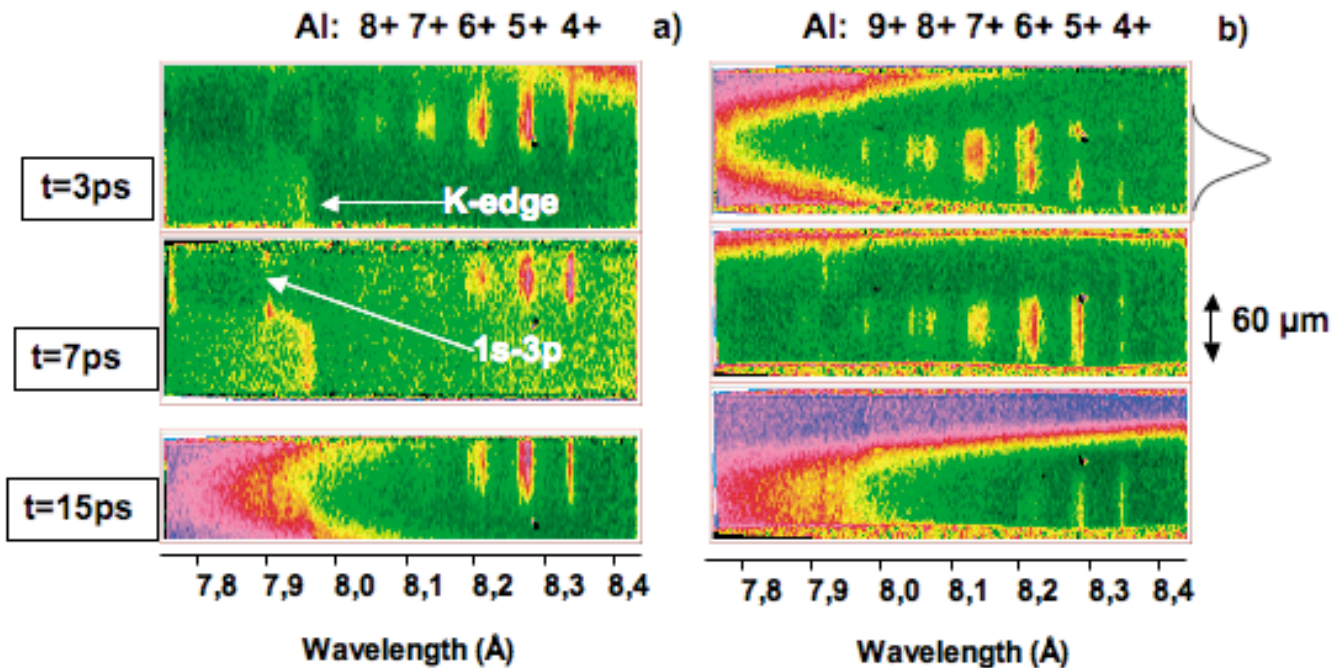
FIG. 2 (color). Space-resolved absorption lines obtained at three different times after laser peak for two different thicknesses of Al, (a) 83 nm, (b) 50 nm irradiated at a laser intensity of 3×10^{15} W/cm^2. The shadow of the 300-μm diameter gold pinhole (red ellipse), the cold Al K edge at 7.949 Å, and the $1s$-$3p$ Al^{3+} line at 7.883 Å can be seen, together with the spatial shape of the pump laser pulse.
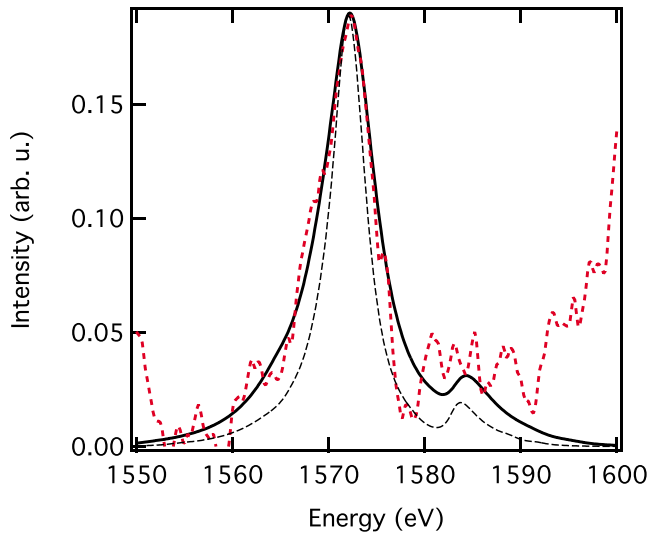
FIG. 3 (color online). Experimental spectrum (dashed line) of the $1s$-$3p$ line of Al^{3+} obtained during the laser pulse, compared to the prediction of the TOTAL code at $N_e = 5 \times 10^{22}$ cm^{-3} (solid line), $N_e = 3 \times 10^{22}$ cm^{-3} (thin dashed line), and $T_e = 50$ eV.

FIG. 4.   Transmission, 7 ps after the heating pulse, of a 83-nm Al foil heated at a laser intensity of 3×10^{15} W/cm^2 (dashed line). The best HULLAC/GA fit is shown for comparison (solid line).

velocity of the critical surface, which is related to the electron temperature [10]. This parameter can be inferred with a self-similar 1D isothermal expansion model of the plasma, assuming a uniform initial density equal to solid density, a Thomas-Fermi equation of state, and an initial electron temperature, which is therefore the only unknown parameter. The self-similar model assumptions were cross-checked by hydrodynamic simulations run with the code MULTI-FS [12]. For the two foil thicknesses, the best fit of the measured phase, for a laser intensity of 3×10^{15} W/cm^2, was obtained for an initial temperature of 50 ± 5 eV. This value is the temperature assumed to be achieved at the peak of the foil heating pulse.

The analysis of an absorption spectrum recorded at a timing near the peak of the heating pulse ($t = 0.3$ ps) indicates that the plasma density remains high. The Al^{3+} $1s$-$3p$ linewidth (83-nm foil) is mostly due to Stark broadening, which is highly dependent on the electron density. In Fig. 3 is plotted the lineout of the experimental Al^{3+} line superimposed with two calculations obtained with the TOTAL/PPP code [13], taking into account Doppler and instrumental broadening. The electron temperature was assumed to be the 50-eV inferred from the FDI diagnostic. A minimum value of the ion density of about 0.25 times solid density can be inferred from the best fit electron density of 5×10^{22} cm^{-3} since the average ionization is lower than 4 (no Al^{4+} absorption line was visible at that time). Unfortunately, the $1s$-$2p$ transitions are not Stark broadened enough to provide a density diagnostic in the focal spot at later times (see Fig. 2).

Each absorption spectrum obtained for a specific time at the center of the focal spot was analyzed using the HULLAC
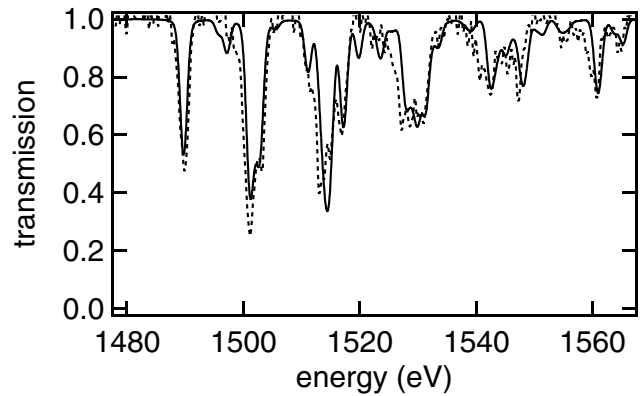
code [14], while the ion charge distribution was determined by a genetic algorithm (GA) procedure [15]. The relative populations of all ionic states between charges 4+ and 9+ were encoded in a 30-bit binary "chromosome." A population of 100 chromosomes was found sufficient for the algorithm to run accurately and rapidly. Figure 4 shows a typical lineout measured for a 50-nm foil, and the best HULLAC/GA fit. The ion distribution is relatively large due to the temporal variation of plasma parameters during the finite duration of the backlighter pulse. All the spectra were analyzed using the same method, providing the time evolution of the average ionization, as shown in Fig. 5, for (a) the 83-nm thick Al foil and (b) the 50-nm foil. Error bars on the time scale have been determined by the finite duration of the backlighter and by the uncertainty in the "zero time" of the experiment, when the pump laser and the x-ray probe are simultaneous. Vertical error bars for the lower average ionization data arise mostly because the $Z = 3$ ion stage does not have any spectroscopic signature in
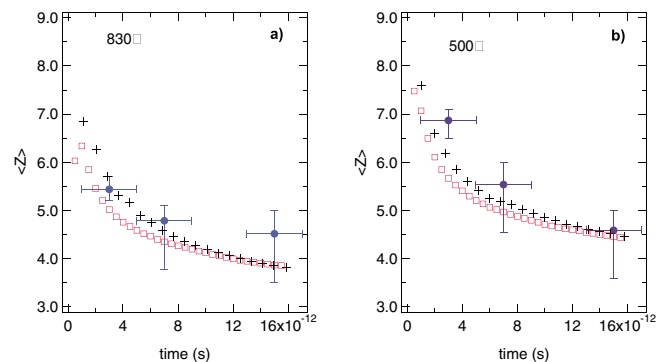
FIG. 5 (color online). Time evolution of the measured average ionization of (a) 83 nm and (b) 50 nm Al foils compared to the numerical simulations of the areal-mass-weighted average ionization under LTE (crosses) and non-LTE (open squares) conditions.

$1s$-$2p$ absorption. The electron temperature is expected to be higher, on spatial average, in the thinner foil as exhibited by the higher ionization stages observed in the experiment (see Fig. 5).

For comparison with theoretical recombination data, the time-resolved absorption spectra and the evolution of the average charge of the plasma were calculated using the AVERROES-TRANSPEC [16] atomic package as a postprocessor of the 1D hydrodynamic MULTI-FS code [12]. Collisional and radiative rates as well as the mean energies and variances of all the possible electron radiative transitions, including a high number of doubly excited levels of Al ions were first calculated with the AVERROES [16] superconfiguration code. Then, the time-dependent ion populations and the average charge were calculated with the collisional-radiative code TRANSPEC using the superconfiguration code data. For the two foil thicknesses studied, the temporal evolution of the average ionization under non-LTE and LTE assumptions are shown in Fig. 5. The calculated ionization is spatially averaged with a weight given by the areal mass of the cells. We emphasize that the comparison between experiment and numerical simulations is free of parameter tweaking. Indeed, the laser intensity used in the simulation was set to reproduce the measured laser peak electron temperature, and was cross-checked with the measured laser intensity calculated from laser energy and the measured focal spot geometry. The 50-nm foil is hotter than the 83-nm foil at constant deposited laser energy. This explains the higher average charge reached for the 50-nm foil. The highly transient ionization state given by TRANSPEC in LTE is in reasonable agreement with experimental data. The small difference between LTE and non-LTE simulations is explained by the high-density and the relatively low temperature of the plasma, which favor three-body collisional recombination. We note that pressure ionization, which is important in our regime, is a key ingredient in the simulations. The way TRANSPEC deals with this effect—a combination of continuum lowering and reduction of the statistical weights [17]—seems to be satisfyingly accounted for. Finally, characteristic recombination times of medium-charge aluminum ions are rather long, on the order of a few picoseconds.

In conclusion, the picosecond recombination dynamics of a few skin-depth thick Al foils heated with a high-intensity ultrashort laser pulse has been measured using point-projection absorption spectroscopy for the first time to our knowledge. Initial foil thicknesses were checked from measured absorption near the cold K edge. At the peak of the laser pulse, the electron temperature was measured by the FDI diagnostic system, while x-ray K-shell Stark-broadened $n = 1$ to 3 lines provided a determination of the electron and ion density averaged over the finite duration of the backlighter x-ray pulse.

Recombination times of multicharged aluminum ions around $Z = 4$–7 have been directly measured and compared to state-of-the-art supertransition-array collisional-radiative models coupled to hydrodynamic simulations constrained by the measured peak plasma parameters. Our experiment is a significant step towards a better understanding of the intermediate state of matter between solids and plasmas, the realm of warm dense matter.

[1] H. Daido, Rep. Prog. Phys. **65**, 1513 (2002).
[2] J. D. Lindl *et al.*, Phys. Plasmas **11**, 339 (2004).
[3] D. D. Ryutov and B. A. Remington, Plasma Phys. Controlled Fusion **44**, B407 (2002).
[4] R. W. Lee, J. K. Nash, and Y. Ralchenko, J. Quant. Spectrosc. Radiat. Transfer **58**, 737 (1997).
[5] J.-C. Gauthier, in *Atoms, Solids, and Plasmas in Super-Intense Fields*, edited by D. Batani *et al.* (Kluwer Academic/Plenum Publishers, New York, 2001).
[6] A. Forsman, A. Ng, G. Chiu, and R. M. More, Phys. Rev. E **58**, R1248 (1998).
[7] T. S. Perry *et al.*, Phys. Rev. E **54**, 5617 (1996).
[8] C. Chenais-Popovics *et al.*, in *Laser-Generated and Other Laboratory X-Ray and EUV Sources, Optics, and Applications, San Diego, CA, 2003*, SPIE Proceedings Vol. 5196 (SPIE-International Society for Optical Engineering, Bellingham, WA, 2004), pp. 205–212; C. Chenais-Popovics *et al.*, J. Phys. IV (France) **108**, 137 (2003).
[9] M. Fajardo *et al.*, Phys. Rev. Lett. **86**, 1231 (2001); M. Fajardo *et al.*, J. Quant. Spectrosc. Radiat. Transfer **71**, 317 (2001).
[10] J. P. Geindre *et al.*, Opt. Lett. **26**, 1612 (2001); R. Shepherd *et al.*, J. Quant. Spectrosc. Radiat. Transfer **71**, 711 (2001).
[11] E. Martinolli *et al.*, Rev. Sci. Instrum. **75**, 2024 (2004).
[12] K. Eidmann, J. Meyer-ter-Vehn, T. Schlegel, and S. Hüller, Phys. Rev. E **62**, 1202 (2000).
[13] S. Alexiou *et al.*, J. Quant. Spectrosc. Radiat. Transfer **58**, 399 (1997).
[14] A. Bar-Shalom *et al.*, J. Quant. Spectrosc. Radiat. Transfer **71**, 169 (2001).
[15] I. E. Golovkin, R. C. Mancini, S. J. Louis, R. W. Lee, and L. Klein, J. Quant. Spectrosc. Radiat. Transfer **75**, 625 (2002).
[16] O. Peyrusse, J. Phys. B **32**, 683 (1999); **33**, 4303 (2000).
[17] G. B. Zimmerman and R. M. More, J. Quant. Spectrosc. Radiat. Transfer **23**, 517 (1980).